Project

Title: Targeting telomerase using structure-based drug repurposing approach: A therapeutic strategy to investigate anti-cancer potential of FDA approved drugs.

1. Introduction:

Cancer continues to be one of the leading causes of death worldwide, affecting millions of lives and straining healthcare systems. Despite the progress made in cancer therapy, there is still a need for new and efficient therapies that can alleviate critical side effects caused by conventional treatments (Pucci et al., 2019). Cellular immortality as envisaged by upregulated telomerase is an established hallmark of all the cancer cells (Hanahan & Weinberg, 2000). The fact that the enzyme is highly upregulated in more than 85% of cancer malignancies and is undetectable or present in low amounts in somatic cells makes it a remarkable anti-cancer drug target.(Kim et al., 1994; Shay, 1997). Developing drugs that target telomerase still remains a hot area as it gives leverage to selectively disrupt the replication of cancer cells and induce their senescence or death meanwhile sparing the healthy cells.

Recent advances in the structural biology of the enzyme have clearly indicated that telomerase is a large ribonucleoprotein complex, architecturally bilobular in shape. The catalytic core is made of the TERT ribonucleoprotein complex and H/ACA lobe-ribonucleoprotein complex is majorly involved in non-canonical roles of the enzyme (Nguyen et al., 2018). TERT, along with the shelterin complex of proteins, uses TERC as a template to add repeats of TTAGGG at the 3'end of the lagging strand of DNA, thereby circumventing the hayflick limit and leading to the evolution of most cancer malignancies (Shay & Wright, 2000; Wright & Shay, 1992). Structurally, the catalytic TERT subunit of the enzyme in humans is mainly composed of four subunits, which are ordered from N-terminal to C-terminal as: TEN, TRBD, RT, and THUMB domains. The last three subunits form a TERT ring structure where the RNA template TERC integrates (Robart & Collins, 2011). (**Figure.1**)

Targeting either of the two telomerase subunits (TERT or TERC) has been the goal of anticancer medicine. Many telomerase-based therapies and drugs based on different mechanisms are currently under investigation. The most successful is the 13-mer modified oligonucleotide GRN163L (Imetelstat), which is in Phase I and Phase II clinical trials for multiple cancer subtypes. Other classes of inhibitors in trials include G-quadruplex stabilizers, heat shock protein90 (HSP90) inhibitors, and tankyrase inhibitors. Furthermore, the development of telomerase-specific immunotherapies, such as telomerase peptide vaccines or adoptive T-cell therapies, has gained attention as alternative strategies to target telomerase in cancer cells. (Guterres & Villanueva, 2020). Despite extensive efforts and time taken, none of the small molecule telomerase inhibitors have been clinically approved yet. A highly selective small molecule telomerase inhibitor, BIBR1532 is still in the pre-clinical stages due to cytotoxicity issues (Ding et al., 2019). Likewise, other small molecule inhibitors like MST-312, TMPI, and costunolide. are in preclinical stages only (Vishwakarma et al., 2023).

Thus, cancer treatment has opened a great avenue for preclinical and clinical development of small molecule telomerase inhibitors because of their low molecular weight, ease of oral

administration, low cost, and ability to pass through cell membranes to reach intracellular targets.

Development of telomerase inhibitors has been hampered by significant challenges, including the lack of structural information despite telomerase being discovered way back in 1984 by Elisabeth Blackburn and Carol Grieder. A major breakthrough in the field came when the crystal structure of the *Tribolium castenum* TERT (tcTERT) bound to a highly specific telomerase inhibitor, BIBR1532 was reported. (PDB ID: 5CQG). This study indicated the specificity of the inhibitor in binding to a conserved hydrophobic FVYL motif in the thumb domain of tcTERT. The FVYL pocket was found to be highly conserved in human TERT, and also as a binding site for the P6.1 AND CR4/5 loops of the RNA template (TERC) (Bryan et al., 2015).

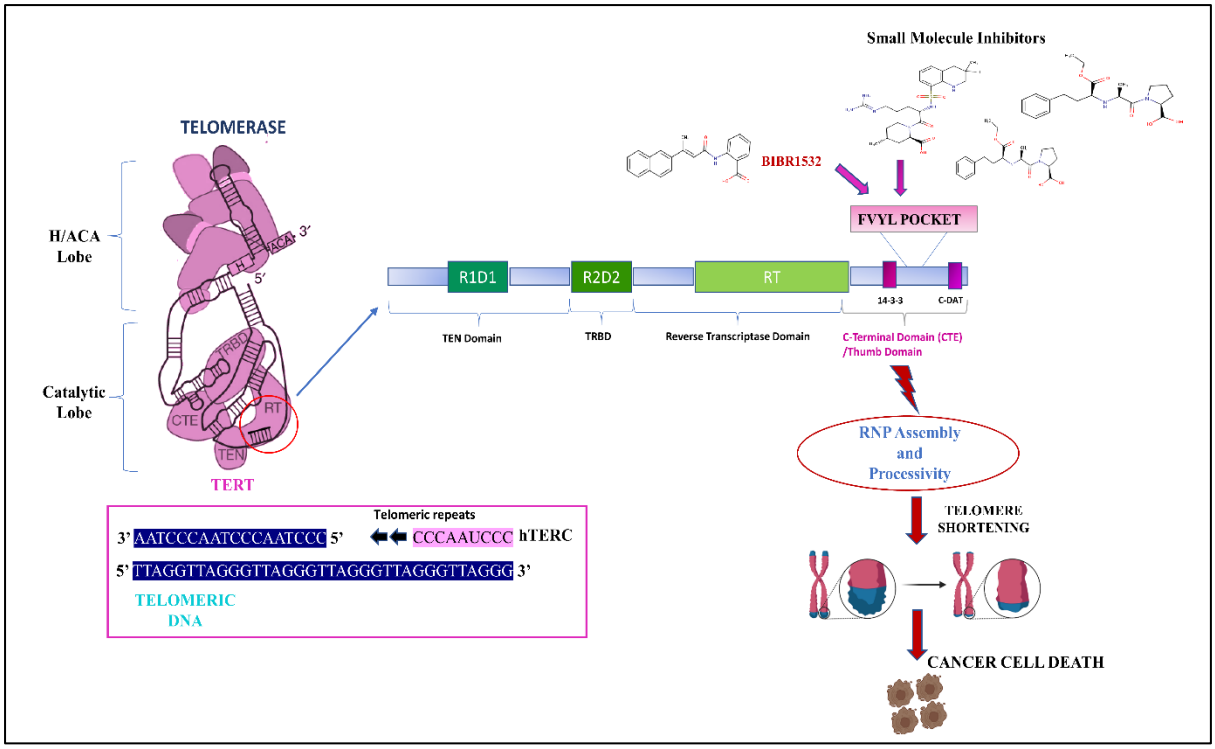

Figure.1: Schematic representation of Telomerase enzyme activity inhibited by small molecule inhibitors binding to hTERT thumb domain will hamper its assembly and processivity to cause cancer cell death. The four domains of hTERT catalytic subunit from N-terminal to C-terminal end i.e TEN, TRBD, RT and CTE/thumb domain are illustrated. (Modified from Ghanim et al., 2021)

Later in 2017, Crystal structure of human telomerase thumb domain was reported from 965 to 1122 residues with 2.61Å resolution (PDB ID:5UGW). The mutational studies performed in this paper provided deep insights into the clinically relevant residues in the thumb domain of the enzyme and their role in a variety of telomeropathies, in addition to confirming that the thumb domain is responsible for the processivity and assembly of the ribonucleoprotein complex. (Hoffman et al., 2017). Thus, targeting thumb domain will hamper the telomerase activity resulting in the cessation of tumour cell replication potential and eventual cell death.

In present day scenario, cues from a literature based on sequence similarity and phylogeny indicate that the BIBR1532 binds to hTERT in the FVYL pocket in the similar manner as tcTERT, disrupting the crucial TERT-TER interaction (Bryan et al., 2015; Hoffman et al., 2017; B. Liu et al., 2022). However, owing to the lack of a co-crystallized structure, it is still not confirmed.

In this study, we have exploited the highly conserved and clinically relevant FVYL pocket in the thumb domain of human telomerase to develop small molecule telomerase inhibitors with the major focus on drug repurposing approach. (**Figure.1**) We first attempted to understand how BIBR1532 binds to the pocket using in silico molecular docking and confirmatory molecular dynamics studies. Subsequently, we followed a structure-based drug design strategy to develop pharmacophore models which have been screened through DrugBank library which contains FDA approved drug molecules. The top hits have been validated using MD simulation studies followed by cross-validation studies using binding free calculations using MM-PBSA and MM-GBSA analysis. Currently, the selected drugs are being used for the treatment of different diseases, and their targets have been elucidated. We have identified five drugs showing considerable telomerase inhibition and proposed that they can be repurposed for the treatment of cancer as a standalone therapy or at least as a second line of defence after the initial debulking of tumours by chemotherapy and radiotherapy. This brings a new therapeutic perspective to already existing drugs in market in a cost effective and time saving manner.

2. Objectives

- To investigate the potential of thumb domain of Telomerase enzyme as a therapeutic target.
- To generate the structure-guided pharmacophore model for the thumb domain of telomerase enzyme using BIBR1532 as a reference molecule.
- To identify hit compounds from DrugBank Approved and Investigational database using virtual screening approach as potential telomerase inhibitors.
- Elimination of false positives by secondary screening using various drug likeliness parameters like ADME and Lipinski rule of five, and TOPKAT toxicity prediction.
- To funnel down the lead molecules using molecular docking technique and interaction with critical residues in hTERT thumb domain and shortlisting the lead compounds based on binding energy scores and their biological mode of action.
- Validation of stability of selected lead compounds using molecular dynamics and binding free energy studies using MM-PBSA and MM-GBSA.

3. Materials and methods

3.1 Protein preparation and binding site identification in hTERT

The crystal structure of Tribolium castenum TERT (tcTERT) co-crystalized with BIBR1532 (PDB ID:5CQG) and human telomerase thumb domain (PDB ID:5UGW) having resolution of 2.30 Å and 2.31 Å respectively, were retrieved from protein data bank (PDB) (Bryan et al., 2015; Hoffman et al., 2017). Protein structures were first prepared in Biovia Discovery Studio (DS) 2020 using the Prepare protein module to add missing hydrogen atoms and loops. All water molecules were removed from the structures. The thumb domains of tcTERT and hTERT were aligned and superimposed in Biovia DS 2020 following the sequence alignment studies reported on the basis of structural and sequence similarity (Bryan et al., 2015). Based on literature study, hydrophobic FVYL pocket located in hTERT thumb domain was identified to be exploited in this study. BIBR1532 was also docked in this hydrophobic pocket and validated it using CDOCKER, Libdock and flexible docking modules available in DS Studio 2020.

3.2 docking of BIBR1532 in FVYL pocket of hTERT

The hydrophobic FVYL pocket was located in hTERT thumb domain by superimposition studies and was defined as the binding site sphere for docking studies. BIBR1532 was extracted from the tcTERT structure, and energy was minimized using the steepest descent method (2000 steps), followed by the conjugate gradient method (2000 steps) using the energy minimization tool of Biovia DS 2020. The ligand was docked into the FVYL pocket using LibDock which is a high-throughput hotspot-based docking module wherein both the receptor and ligands are rigid. Alternatively, BIBR1532 was also docked using molecular dynamics based simulated annealing CDOCKER protocol available in DS 2020 (Rao et al., 2007; Wu et al., 2003). Finally, the docking was performed using a flexible docking module which allowed both the receptor and ligand to be flexible with the highest level of accuracy (Rarey et al., 1996). The active site residues (Q1024, V1025, W1026, V1087, T1088, Y1089, L1090) were made flexible to dock BIBR1532 into the binding site.

3.3 In-situ ligand minimization of BIBR1532 in FVYL pocket and MD simulation

Owing to the undesired results, the methodology was improvised. BIBR1532 was placed in putative FVYL pocket and in-situ ligand energy minimization was carried out. The in-situ ligand minimization protocol minimizes the ligand in the presence of a rigid receptor. However, residues with atoms inside the specified binding sphere or flexible residues are allowed to move. A Molecular Dynamics (MD) simulation run of 20ns in the CHARMm36 forcefield was performed to confirm the stability of the ligand in the pocket.

Protein topology of the complex was generated using pdb2gmx module in the CHARMm36 force field using Gromacs 2020.1 package in the linux environment. The ligands were fully hydrogenated using Avogadro software before generating their topology using an external CGenFF server (Hanwell et al., 2012; Vanommeslaeghe et al., 2010). The protein-ligand complex was then solvated using the TIP3P water model in a cubic box, which defined its periodic boundary conditions. a cubic box and minimized using the steepest descent algorithm. Suitable concentrations of Na^+ and Cl^- ions were added to the solvated system to neutralize the charges, followed by energy minimization using the steepest descent algorithm (50000 steps). The energy-minimized complex was equilibrated under NVT and NPT (constant number of particles, volume, temperature, and pressure) conditions for 100ps each. The bond lengths were restrained using LINear Constraint Solver (LINCS) algorithm and long range electrostatics were calculated using the particle mesh Ewald (PME) method (Essmann et al., 1995). Short-range interactions were computed using a van der Waals cutoff at 1.2 nm (Vařeková et al., 2004).
A final MD run of 20ns was then performed and snapshots were saved for every 10ps frame. Trajectory analysis was performed post MD and graphs were extracted for RMSD, RMSF and Ligand RMSD specifically. Last 5% of the MD simulation trajectory was manually analyzed to screen out the best pose with the lowest RMSD and maximum set of required interactions using PyMOL and Biovia DS 2020

3.4 Revalidation of the binding site of BIBR1532 by redocking

To ensure that BIBR1532 binds well onto the newly observed pocket. The selected protein-ligand complex pose from the 20ns MD simulation was exported into the Biovia DS 2020 and the site binding sphere was defined at the exact pose with coordinates X= 61.148 Y=61.587 Z= 30.441 from the define and edit binding site tool in DS. The ligand was prepared and docked onto this binding site using the CDOCKER module.

3.5 Structure-based pharmacophore generation

Given that the FVYL pocket is a highly conserved cavity, structural investigations continue to indicate that BIBR1532 must also bind to it in the thumb domain of the human telomerase (B. Liu et al., 2022). However, this is still uncertain due to the lack of availability of the inhibitor's co-crystallized structure with hTERT. Consequently, structure-based pharmacophore models were generated following a two-way approach. A pharmacophore is a set of steric and electronic features extracted from a binding site of a ligand bound to a protein in a complex. It can be used as a framework to search for ligands similar to an already known selective inhibitor, whose binding site is known.
In the first approach, Pharmacophore models was generated from the pose wherein BIBR1532 was placed in FVYL pocket and in-situ ligand minimized, using Receptor-Ligand pharmacophore Generation (RLPG) module in Discovery studio 2020. Excluded volumes were automatically generated to prevent steric clashes.

In another approach, pharmacophore models were generated from a selected pose with the least RMSD and maximum interactions in the last 5% of the 20ns MD simulation trajectory.
Finally, the pharmacophore model with the required feature set and highest selectivity score predicted by genetic function approximation (GFA) was selected from the set of pharmacophores generated by both approaches, as described. The models were named Pharmacophore_A1 and Pharmacophore_B1, corresponding to the two different pockets from which they were generated.

3.6 Validation of pharmacophores

A well-validated pharmacophore virtually screens out molecules with chemical properties equivalent to or better than the control ligand, ensuring high specificity and selectivity to the binding site (X. Liu et al., 2010).
The control ligand BIBR1532 was mapped onto pharmacophore models A1 and B1 using the ligand-pharmacophore mapping protocol of Biovia Discovery Studio 2020. This was performed to obtain a standard fit value for the control ligand with the pharmacophores. The fit value of the control BIBR1532 was subsequently used as a cut-off to filter top hits from a virtually screened set of DrugBank compounds.

3.7 Pharmacophore-based virtual screening

The goal of building pharmacophore models is to search for multiple ligands that can bind to the same receptor with high selectivity and sensitivity. High-throughput virtual screening (HTVS) is crucial to the in-silico drug discovery process because it enables quick and inexpensive screening of compound libraries that are substantially larger than those that can be screened experimentally, thereby accelerating the drug development process.
Both pharmacophore models were virtually screened through the entire DrugBank approved and investigational database with a total of 2509 and 3589 compounds, respectively, using the screen library module and FAST method of conformation generation in Biovia DS 2020. Initial funnelling of hits was performed based on the cut-off fit value of control BIBR1532, i.e fit value ≥ 3.6 and ≥ 2.8 for pharmacophore models A1 and B1, respectively.

3.8 PK properties filtering

DrugBank is a richly annotated, freely accessible database of FDA-approved and investigational drugs, among many other sets of compounds, with a comprehensive amount of information about the pharmacodynamics (PD) and pharmacokinetics (PK) of each drug. This database was used in our study, with a targeted focus on drug repurposing.

The DrugBank approved set contains compounds officially accepted for commercialization and thus has passed the check of all drug-likeliness parameters. In contrast, the DrugBank investigational set contains drugs being researched for determinate conditions and has reached clinical trials and thus is yet to pass PD and PK studies (Wishart et al., 2008).
We applied the ADME and TOPKAT tools available in Biovia DS 2020 to filter hit compounds obtained from the screening DrugBank Investigational dataset using both the Pharmacophore_A1 and Pharmacophore_B1 models.
In Computer-aided drug design (CADD), the computational characterization of drug likeliness properties, such as Adsorption, Distribution, Metabolism and, Excretion (ADME), and toxicity prediction are of vital importance as they reduce the likelihood of rejection in clinical development. These properties influence the dosing, benefits, and adverse effects of drugs (Meibohm & Derendorf, 1997).

3.9 Molecular docking

Validation of hit compound binding in the two identified pockets corresponding to each pharmacophore model was a crucial step in our study. Filtered ligands from DrugBank approved and investigational databases were prepared, and energy was minimized using the steepest descent method (4000 steps) followed by the conjugate gradient method (4000 steps). The first binding-site grid was defined at the putative FVYL pocket identified from superimposition studies corresponding to Pharmacophore_A1, using the Define and Edit tool of Biovia DS 2020. The filtered ligands were docked onto this site in hTERT (PDB ID:5UGW) using the CDOCKER module available on Biovia DS 2020.
A second binding site grid was defined at the pose selected after the 20ns MD simulation study corresponding to Pharmacophore_B1. The prepared ligands from each database were docked similarly onto this site in hTERT as well.
CDOCKER, as discussed previously, is a molecular dynamics-simulated-annealing-based docking protocol that employs the CHARMm force field to accurately dock ligands flexibly into the rigidly held receptor protein (Gagnon et al., 2016; Wu et al., 2003). Top hits from the DrugBank approved database were chosen as candidates for further Molecular dynamics studies and experimental validation.

3.10 Molecular dynamics simulations and analysis

Molecular dynamics (MD) simulations were performed to ascertain the stability of the chosen candidate molecules in the presence of hTERT receptor interacting for a brief amount of time at the atomic level.
The selected top five hit molecules from DrugBank approved database i.e DK1_DRUG, DK2_DRUG, DK3_DRUG, DK4_DRUG and DK5_DRUG alongside the control BIBR1532, in complex with hTERT thumb domain were subjected to a 100ns MD run using Gromacs 2020.1 package with CHARMm36 forcefield using the same methodology as discussed in detail in section 2.3. (Brooks et al., 2009).

Trajectory analysis was performed after MD simulation in PYMOL software, and graphs for root mean squared deviation (RMSD), root mean square fluctuation (RMSF), and Radius of Gyration (RoG) were extracted for all ligand-protein complexes using Gromacs tools (gmx rms, gmx rmsd, gmx gyrate) on the Linux platform. Comparative graphs were plotted using the Grace software to understand the stability of the top five drug hits with respect to the control ligand in the hTERT thumb domain (*Grace Home*, n.d.). The crucial FVYL pocket interactions were evaluated in Biovia DS 2020 after the MD Simulation.
RMSD graph indicates fluctuation of the protein backbone atoms in the presence of all the drugs in a binding pocket with respect to time. In contrast, the RMSF graph shows individual residue fluctuations over the simulation period. The RoG graph is a measure of how well the protein structural compactness remains maintained throughout the simulation trajectory.

3.11 MM-PBSA binding energy calculations

Additionally, revalidation of the MD simulation study was performed by enumerating the binding free energies of the top five selected candidate drugs and BIBR1532 using the gmx_MMPBSA package version 1.4 (Miller et al., 2012; Valdés-Tresanco et al., 2021). We extracted the last 20ns of each MD run (80ns to 100ns) and removed all periodic boundary conditions as a precondition to calculate the Molecular Mechanics Poisson-Boltzmann surface area (MM-PBSA) scores. Analysis was performed using the gmx_MMPBSA_ana pipeline tool.
The binding free energies of the solvated protein-ligand system can be expressed using the following equation:

$$\Delta G_{binding} = \Delta G_{complex} - [\Delta G_{protein} + \Delta G_{ligand}]$$

where $\Delta G_{complex}$ is the receptor-ligand total free energy, and $\Delta G_{protein}$ and ΔG_{ligand} are the isolated total free energies of the receptor protein and ligand, respectively, in a solvent.

The free energy of the ligand-protein complex can be calculated as follows:

$$\Delta G_{binding} = \Delta \mathbf{H} - T\Delta S$$

Or,

$$\Delta G_{binding} = \Delta \mathbf{E_{MM}} + \Delta \mathbf{G_{solv}} - T\Delta S$$

where ΔE_{MM}, $\Delta G_{solv,}$ and $T\Delta S$ are the changes in gas-phase molecular mechanics, solvation energy, and conformational entropy upon ligand binding, respectively.

ΔE_{MM} helps to calculate the bonded and non-bonded interactions using the following equation:

$$\Delta \mathbf{E_{MM}} = \Delta E_{bond} + \Delta E_{vdv} + \Delta E_{elec}$$

Where ΔE_{bond} corresponds to internal energy component of the system and ΔE_{vdv} and ΔE_{elec} are the van der Waals and electrostatic interaction energies, respectively, corresponding to the nonbonding interactions in the MM force field parameters.

The solvation energy has polar and nonpolar components, which can be estimated using the following equation:

$$\Delta G_{solv} = \Delta G_{Polar} + \Delta G_{Non\text{-}polar}$$

Or,

$$\Delta G_{solv} = \Delta G_{PB/GB} + \Delta G_{SA}$$

The polar contribution was estimated using both the Poisson Boltzmann (PB) model and the Generalized Born (GB) model. (Wang et al., 2019). The nonpolar component of the system is usually estimated using the solvent-accessible surface area (SASA). Entropy (ΔS) has a minimal effect on the total energy; hence, it can be neglected.

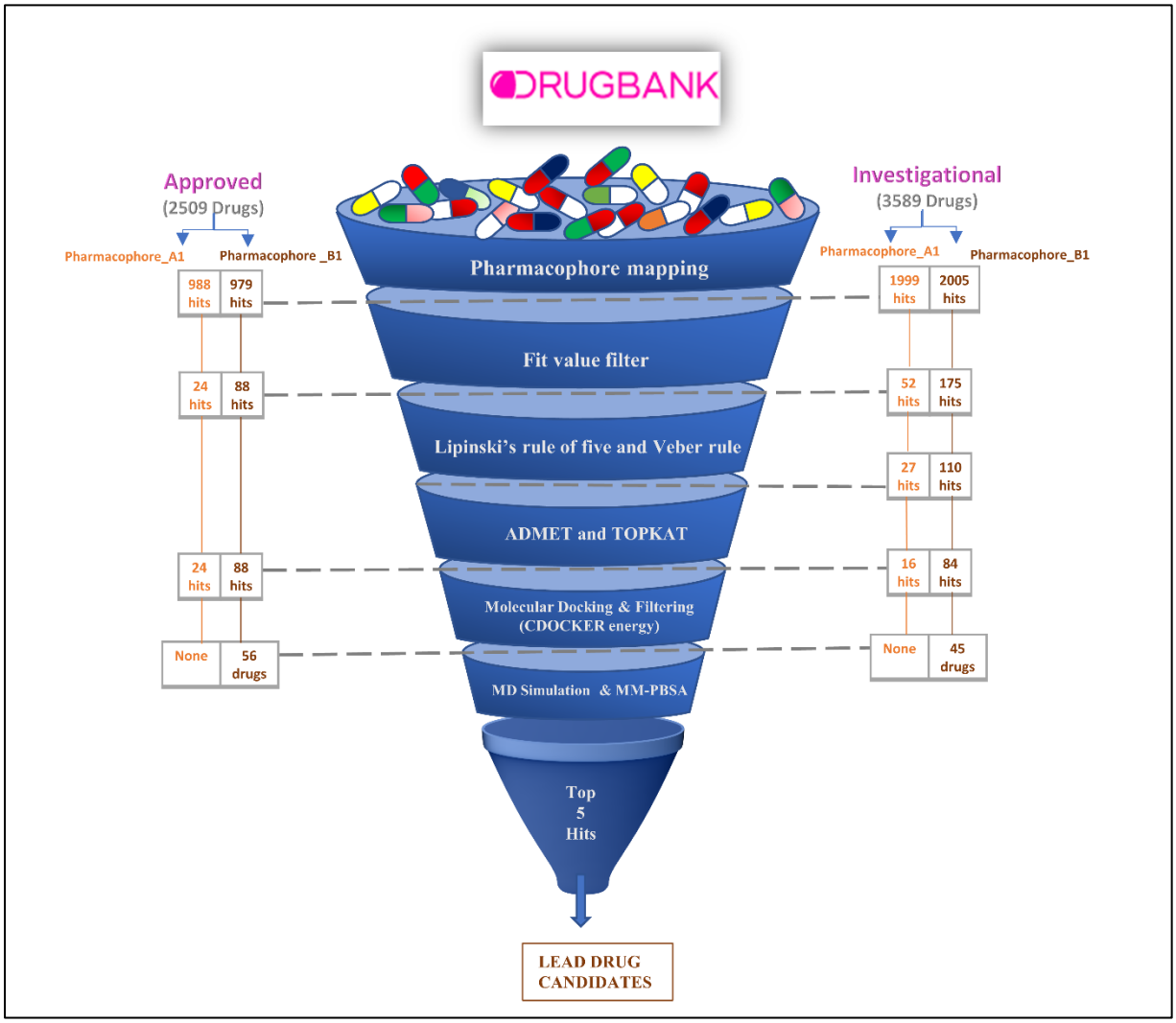

Figure.2: Pipeline for discovery of lead compounds after generation of structure-based pharmacophore.

4. Results

4.1 Binding site identification in hTERT

Structural superimposition of the tcTERT and hTERT thumb domains showed striking similarity in the amino acid composition of the FVYL pocket, as reported in the literature (Bryan et al., 2015). However, the backbone RMSD of the thumb domain was observed to be 6.5 Å and that of the FVYL pocket was 2.5 Å. The initial molecular docking of BIBR1532 by Libdock, CDOCKER, and flexible docking failed to dock the ligand into the putative FVYL pocket. Instead, we observed that the ligand docked alternatively into a shallow binding pocket of the thumb domain and we were unable to obtain the required interactions after multiple attempts. After rigorous structural analysis, it was observed that the FVYL pocket in hTERT was not as large as in tcTERT and therefore BIBR1532 was not able to dock on that site by any of the protocols, validating such high RMSD of the domain as well. (**Figure.3**)

Further confirmation was still required as the literature points towards a high possibility of BIBR1532 to bind to the FVYL pocket of hTERT in a manner similar to tcTERT (B. Liu et al., 2022). Thus, putative FVYL pocket was further exploited.

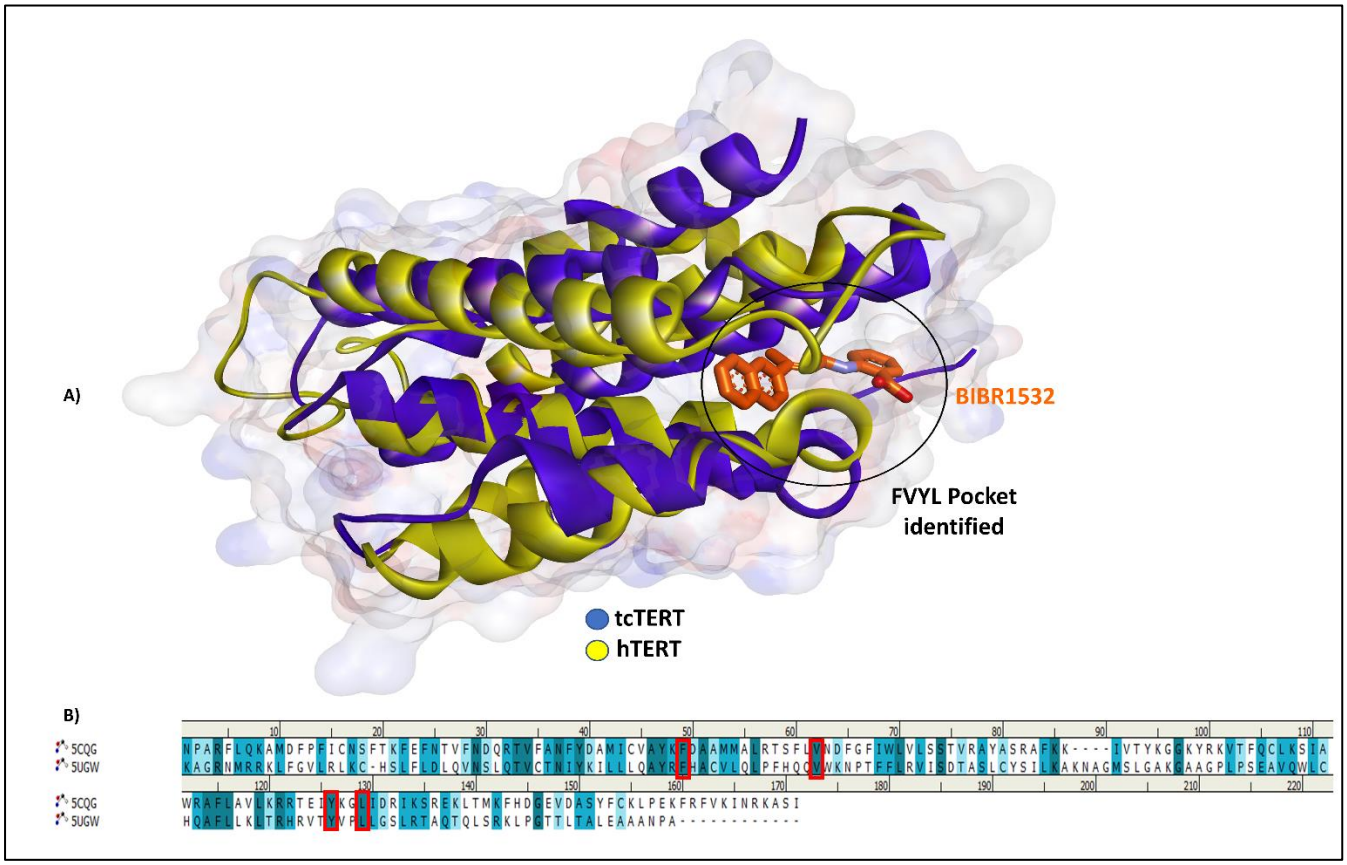

Figure.3 : A) Identification of FVYL binding pocket in hTERT by structural superimposition with tcTERT having co-crystalized BIBR1532 ligand. B) Sequence alignment of tcTERT and hTERT thumb domains. FVYL residues are highlighted in red colour.

4.2 In-situ ligand minimization of BIBR1532 in FVYL pocket and MD simulation

In an improvised methodology, BIBR1532 was placed in the putative FVYL pocket of the human telomerase thumb domain and in-situ energy minimized. Reported thumb domain residues, such as V1016, L1017, F1012, V1025, Y1089, L1092, T1088, and F1032, showed interactions with BIBR1532. Moreover, the in-situ energy drastically reduced from +4.17374e+09 kcal/mol to -552.737 kcal/mol, indicating that ligand was stable inside the pocket.

To confirm the stability of BIBR1532 in this pocket, the complex was extracted in this pose and a 20ns Molecular dynamics (MD) simulation study was carried out.

We observed that the ligand shifted to an adjacent pocket immediately after the NVT equilibration step and remained stable throughout the simulation trajectory in the newly occupied pocket. RMSD, RMSF and Radius of gyration graphs show that the structure remained stable throughout the trajectory. **(Figure.4)**

Poses before and after the MD simulation were superimposed, and it was observed that the new pocket was located approximately 8.491 Å away from the putative FVYL pocket, although the ligand still interacted with most of the important residues and was bound in the same orientation as before. (**Figure.4**) The binding site RMSD was 2.67 Å which is within the appropriate range. It also indicates that the binding site opened up a little to accommodate the ligand, which, however, subsequently remained stable, as observed throughout the trajectory.

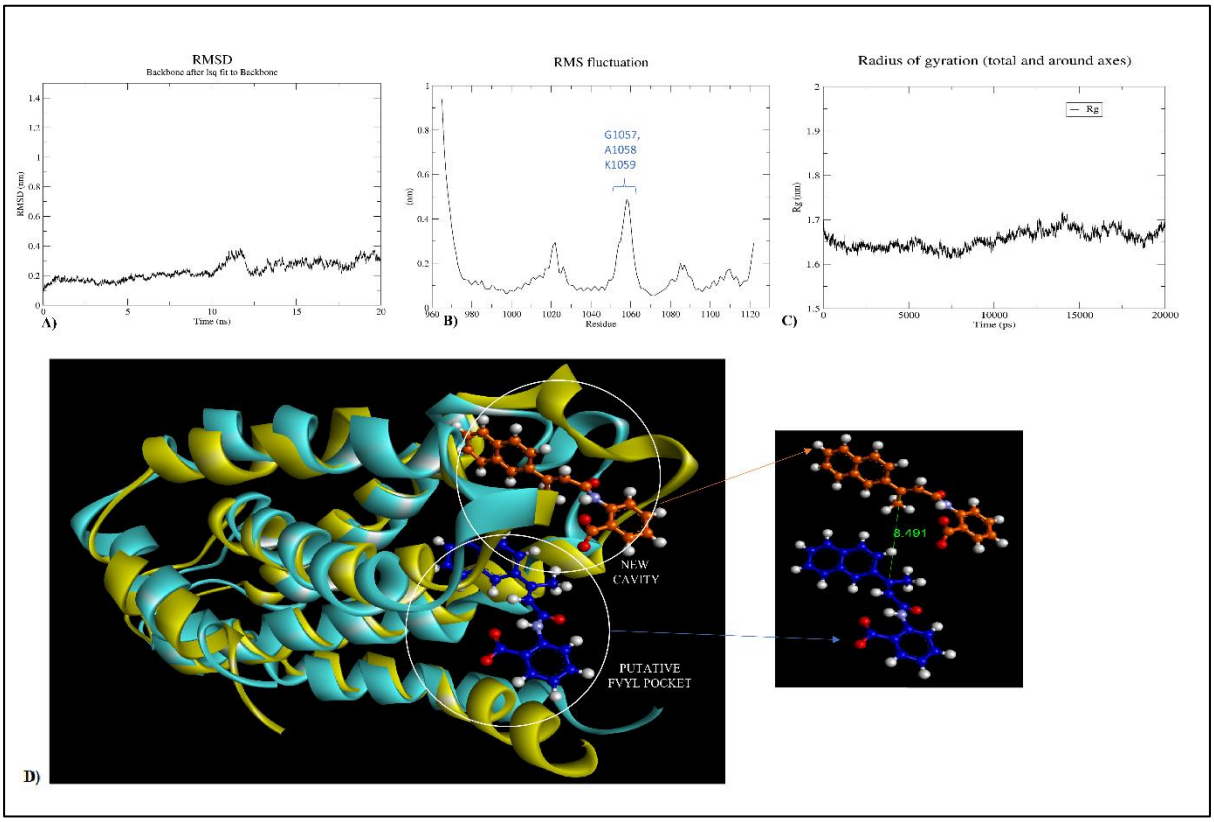

Figure.4: Plots to investigate binding stability of BIBR1532 in putative FVYL pocket after 20ns MD simulation A) represents RMSD B) RMSF C) Radius of gyration D) hTERT thumb domains superimposed before (cyan) and after (yellow) the 20ns MD simulation. A Shift in binding cavity of BIBR1532 from putative FVYL pocket (blue) to a new cavity (orange) 8.491Å away was observed.

4.3 Revalidation of binding site of BIBR1532 by redocking

The validation of BIBR1532 binding affinity into the pocket was critical because the new binding pocket away from the putative FVYL pocket was discovered as a result of an MD simulation study.

BIBR1532 docked successfully into the pocket, revealing the same set of interactions with FVYL and other essential residues as observed after the MD simulation. The observed CDOCKER energy ranged from -11.62 kcal/mol to -7.62 kcal/mol corresponding to ten poses of the BIBR1532 obtained. The negative energy obtained confirmed that the ligand was stable in the binding pocket. This validated that the shift of BIBR1532 from its presumed FVYL pocket to the new pocket was not by chance and that it is most likely its actual binding site.

Additionally, the energy bracket helped us decide a cut-off value at lower limit (-7.62 kcal/mol) to filter the molecular docking results after the screening in later stages.

4.4 Structure-based pharmacophore generation

Structure-based pharmacophore models were generated using a two-way approach in the Biovia DS 2020. We obtained six pharmacophore models from the first approach, where BIBR1532 was placed in the putative FVYL pocket and in situ energy minimization was carried out. Similarly, we obtained ten pharmacophore models from the second approach, wherein the pharmacophore was generated from the selected pose after a 20ns MD simulation run. (**Figure.5** and **Table.1**)

In approach one, the pharmacophore with the highest selectivity score of 7.1958 and feature set AAHHH (two hydrogen bond acceptors and three hydrophobic groups) was selected (Pharmacophore_A1 in **Table.1A**). In the second approach, the top two pharmacophore models had a similar selectivity score of 9.1336, which was the highest. However, the critical distinguishing factor was their feature set (Pharmacophore_B1 in **Table.1B**). We purposely chose a pharmacophore model with the feature set AHHNR (one hydrogen bond acceptor, two hydrophobic groups, one negative ionizable group, and one ring aromatic feature) in contrast to AHHHN. (**Figure.5**) This choice was made with respect to the previously reported mode of interaction of BIBR1532 in the 3D space of the binding site within the prot ein (Bryan et al., 2015). The aromatic ring group of BIBR1532 is an essential contact point between the ligand and protein, making it an essential feature for choosing the correct pharmacophore model.

The selected pharmacophore models A1 and B1, corresponding to the two possible binding sites of BIBR1532 with the highest selectivity scores and suitable feature sets, were subsequently used as queries for virtual screening. A good pharmacophore model is sensitive enough to identify potential novel ligands that can bind to a pocket and are selective enough to avoid false positive candidates. This is possible only by controlling the number of features that must be possessed. A pharmacophore model with 4-6 features is usually considered good, as in our case (Kant et al., 2022).

4.5 Validation of Pharmacophores

Validation of pharmacophore is an important step to determine the fit value by which filtering of top hits should be performed after virtual screening.

This fit value is indicative of how well the features in the pharmacophore map match the chemical features present in BIBR1532 while keeping track of the excluded volume. When BIBR1532 was mapped onto the two pharmacophore models, we obtained a cut-fit value of 3.65 and 2.85 for the model A1 and B1 respectively.

This fit value was subsequently used as a cut-off to filter top hits from a virtually screened set of DrugBank compounds by both the pharmacophore models, which should be ideally better than the control inhibitor. (Jha et al., 2022)

Table.1: Selectivity score and characteristic features of pharmacophores generated **a)** by first approach (A1 to A6) **b)** by second approach (B1 to B10)

Pharmacophore	Number of Features	Feature set	Selectivity score
Pharmacophore_A1	5	AAHHH	7.1958
Pharmacophore_A2	4	AHHH	5.6810
Pharmacophore_A3	4	AHHH	5.6810
Pharmacophore_A4	4	AAHH	5.6810
Pharmacophore_A5	4	AAHH	5.6810
Pharmacophore_A6	4	AAHH	5.6810

A)

Pharmacophore	Number of Features	Feature set	Selectivity score
Pharmacophore_B1	5	AHHNR	9.1336
Pharmacophore_B2	5	AHHHN	9.1336
Pharmacophore_B3	4	HHNR	7.9596
Pharmacophore_B4	4	HHHN	7.9596
Pharmacophore_B5	4	AHNR	7.9596
Pharmacophore_B6	4	AHHN	7.9596
Pharmacophore_B7	4	AHNR	7.9596
Pharmacophore_B8	4	AHHN	7.9596
Pharmacophore_B9	4	AHHN	7.9596
Pharmacophore_B10	4	AHHR	5.7496

B)

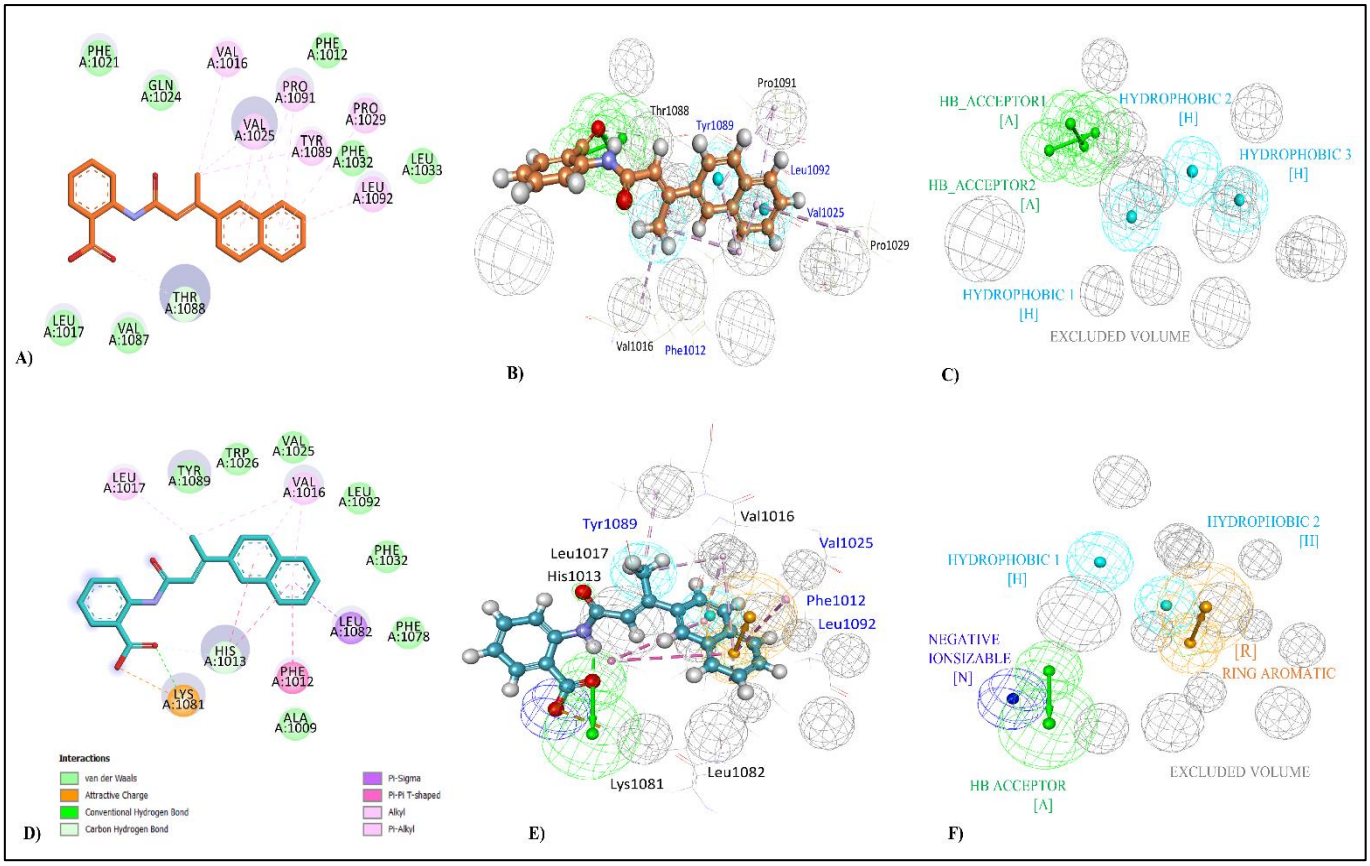

Figure.5: Structure based pharmacophore models selected from approach 1 (A-C) and approach 2 (D-F). A) 2D interaction diagram of BIBR1532 in-situ energy minimized in FVYL pocket B) Pharmacophoric features in the binding pocket C) Best pharmacophore model A1 with feature set AAHHH D) 2D interaction diagram of BIBR1532 in the new pocket after 20ns MD simulation E) Pharmacophoric features in the new binding pocket F) Best pharmacophoric model B1 with feature set AHHNR

4.6 Pharmacophore-based virtual screening

Structurally novel and potential lead molecule identification from diverse chemical databases is possible by high throughput virtual screening (HTVS) of the generated pharmacophore models. The best pharmacophore models A1 and B1 from each approach were screened against a total of 2509 DrugBank approved compounds and 3589 DrugBank investigational compounds.

As a result of the key interaction in the two pockets, 988 and 979 DrugBank approved compounds were mapped to pharmacophore models A1 and B1, respectively. They were filtered based on the fit values of ≥ 3.6 and ≥ 2.8, respectively, resulting in 24 and 88 drugs in each case.

In the case of the DrugBank investigational database, 1999 and 2005 hits mapped to pharmacophore models A1 and B1 respectively. They were also filtered based on similar fit values to arrive at 52 and 175 hits from pharmacophore models A1 and B1, respectively. (Refer **Figure.2** flowchart)

4.7 PK properties filtering

Pharmacokinetics (PK) study involves the study of the absorption, distribution, metabolism, and excretion (ADME) of drugs in the body. Determining the PK properties is a crucial step in drug development process in order to maximise drug efficacy and safety, optimise dosage regimens, and reduce the likelihood of failure in subsequent stages of the process.

DrugBank-approved database is a collection of FDA-approved drugs that have passed all stages of clinical trials, validating the pharmacokinetic properties needed, and falling into the category of de-risked compounds. Thus, drug-likeliness filters such as ADMET, Lipinski's rule of five, and Veber's rule were not applied to them. In contrast these filters were applied to the screened DrugBank investigational compounds to funnel them further.

The ADME tool in Discovery studio helps to eliminate compounds with unfavourable features in terms of human intestinal absorption, blood brain barrier penetration, hepatotoxicity, aqueous solubility, CYP2D6 binding, plasma protein binding and undesired functional groups.

In case of pharmacophore model A1, only 27 out of 52 drugs did not violate Lipinski and Veber rules. Ten of these eventually failed the ADMET parameters.

Finally, after TOPKAT filtering, only 16 molecules remained, with one compound being filtered out as mutagenic. TOPKAT® (TOxicity Prediction by Komputer Assisted Technology) tool in Discovery studio helps to assess ames mutagenicity of compound with cues from its 2D structure alone (Kant et al., 2022).

In case of pharmacophore model B1, 66 out of 175 compounds failed Lipinski's rule of five and Veber's rule, leaving only 110 compounds. Only 96 out of 110 passed the ADME filter, of which only 84 passed the toxicity prediction test using the TOPKAT protocol in Biovia DS 2020.

As a result, we were left with only 84 drug-like and non-mutagenic compounds from the DrugBank investigational database screening from pharmacophore model B1. (**Figure.2**)

4.8 Molecular docking

Molecular docking is a very important part of structure-based drug discovery pipeline. It helps to determine the binding affinity of a particular ligand to a receptor molecule based on a ligand placement algorithm and scoring each pose in which the ligand docks successfully to a protein.

All the top hits from DrugBank approved and investigational databases when docked onto the pocket corresponding to the Pharmacophore_A1 showed unfavourable bumps with the most critical residues in the FVYL pocket.

Critical examination revealed that residues VAL1025, TRP1026, PRO1029, THR1088, TYR1089 and PRO1091 of hTERT protrude inside the putative FVYL pocket, decreasing the effective volume of the cavity and making it impossible for any small

molecule inhibitor from the entire DrugBank library to dock there. These residues showed steric clashes with the placed BIBR1532, making it impossible to dock inside the pocket whereas the corresponding residues in tcTERT keep the pocket open and accessible. (**Figure.6**)

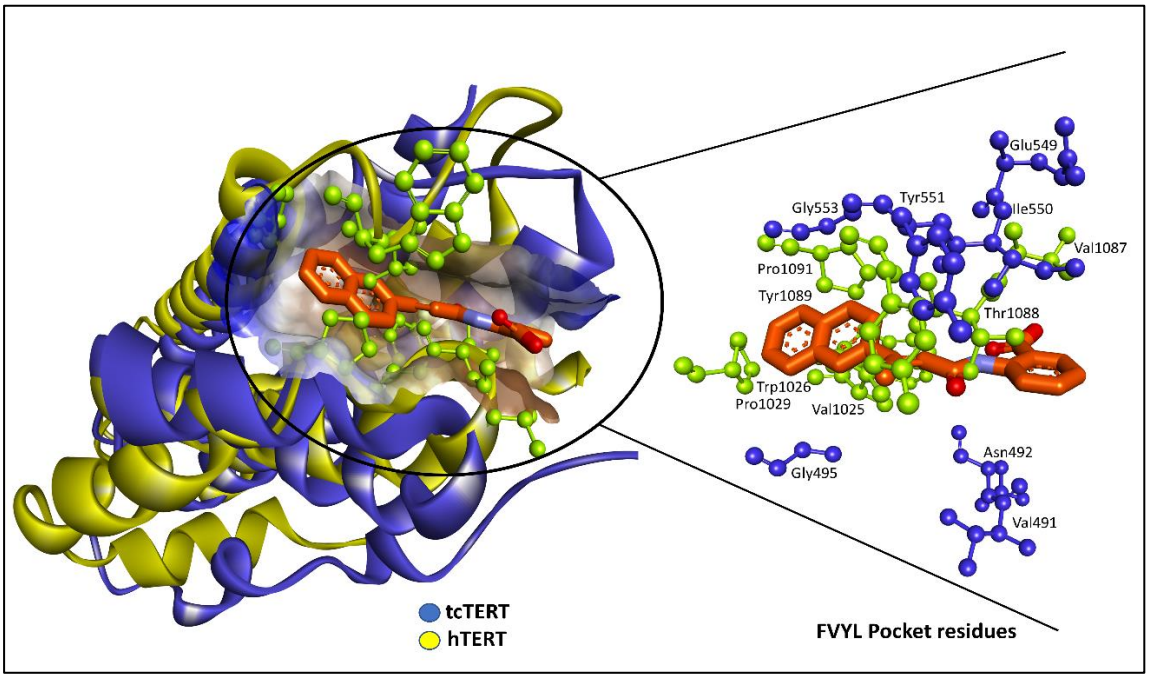

Figure.6: Structural superimposition of tcTERT and hTERT with BIBR1532 in FVYL pocket. Labelled residues of hTERT (yellow) protrude inside the FVYL pocket decreasing the effective pocket volume whereas tcTERT residues (blue) keep the pocket in open conformation.

In contrast to this, ligands from both the databases could easily dock into the pocket corresponding to the Pharmacophore_B1. This pocket though 8.491Å away from the putative FVYL pocket in fact showed almost all essential FVYL interactions in addition to other interactions as well. The top ligands from DrugBank approved as well as investigational databases were filtered on the basis of CDOCKER energy more negative than that of the positive control BIBR1532. (-7.62 kcal/mol)

Molecular docking of 88 ligands from DrugBank approved database and 84 ligands from DrugBank investigational database produced 849 and 850 conformations respectively. We were left with only 56 drugs and 45 drugs after filtering them on the basis of CDOCKER energy from each database.

The Top five hits from the DrugBank approved database i.e DK1_DRUG, DK3_DRUG, DK4_DRUG, DK5_DRUG and DK2_DRUG were chosen as lead candidates for further study based on their interaction with critically important residues of the thumb domain and specifically the FVYL pocket identified through a literature study. The mechanism of action of each drug was thoroughly studied in the context of their possible anti-cancer role and cross-talk with other pathways.

Table.2: Top five DrugBank Approved compounds with their properties.

S.No	Generic Name	Primary Use	-CDOCKER Energy Score	Fit Value
1.	DK1_DRUG	synthetic thrombin inhibitor used for the prevention and treatment of thrombosis related to heparin use.	45.5821	3.49468
2.	DK2_DRUG	Folate analog-thymidylate synthase inhibitor used in the treatment of advanced colon cancer.	40.0942	3.54204
3.	DK3_DRUG	ACE inhibitor used to treat hypertension and congestive heart failure	31.2079	2.96993
4.	DK4_DRUG	Spleen tyrosine kinase inhibitor used to treat chronic immune thrombocytopenia	29.1347	3.29389
5.	DK5_DRUG	Lipoxygenase inhibitor used for the treatment of actinic keratoses	28.8508	2.91418

#Top five lead drugs identified from DrugBank are abbreviated as DK1-DK5 and their exact names are not yet revealed in this report as the manuscript is under preparation.

4.9 Molecular dynamics simulations

Molecular dynamics was performed for 100ns using an explicit solvent model to get further insights into the stability and dynamic behavior of these drugs inside the newly discovered binding pocket in thumb domain of hTERT. It helped us to gain a comprehensive understanding of the behavior of the five lead drugs in comparison to the control ligand BIBR1532 based on metrics like Root mean squared deviation (RMSD), Root mean squared fluctuation (RMSF), Radius of gyration (RoG) and hydrogen bonds formed between protein and ligand throughout the trajectory.

RMSD plot for backbone atoms of the protein in the presence of each drug helped us to assess their structural and conformational stability in the binding pocket with respect to time. All the complexes showed RMSD less than 0.4nm which converged steadily to as low as 0.2nm with time. DK3_DRUG (Blue), DK1_DRUG (Red) and DK2_DRUG (Green) showed a similar trend like the control ligand BIBR1532 (Black). DK4_DRUG (yellow) showed a small deviation between 55ns to 60ns, but it eventually converged towards stability from 60ns onwards. DK5_DRUG also showed a stable trajectory with RMSD averaging near 0.3nm with slight deviations near 30ns and 40ns timepoints, but the complex eventually equilibrated showing a stable trajectory. (**Figure.7A**)

RMSF plot helped us to gain further insights about the flexibility of each amino acid residue of the thumb domain of hTERT in the presence of each drug in the binding pocket.

RMSF values for all the protein-ligand complexes were in the acceptable range. DK1_DRUG, DK3_DRUG and DK5_DRUG showed an average RMSF upto 0.2nm which was even better than the fluctuation seen due to binding of BIBR1532 which had deviation up to 0.28nm near residue P1020, F1021. However, this deviation was still in the acceptable range. DK5_DRUG showed a slight fluctuation in the residues L1056 and K1059 near 0.4nm but these residues were not a part of the binding site.

DK2_DRUG showed fluctuations in the acceptable range for all the residues except F1021 and H1022 and similarly DK4_DRUG showed fluctuations for residues L1056, G1057, A1058 and L1059 which were up to 0.6nm. However, none of these fluctuating residues lie in the binding site of the protein including the FVYL residues. (**Figure.7B**)

We next analyzed the Radius of gyration (RoG) plots extracted from MD trajectories to study the protein compactness and folding dynamics in the presence of the bound drugs. The RoG values of all the complexes were observed to be an average of 1.7nm, being very low and in the acceptable range. All the complexes showed a stable protein-folding dynamics, with their compactness maintained throughout the trajectory. In case of DK4_DRUG, a slight deviation up to 1.85nm was observed, which eventually disappeared as the trajectory converged stably after 60ns. (**Figure.7C**)

Finally, we analyzed the number and duration of hydrogen bonds formed by the five drugs and BIBR1532 in the binding pocket of the protein throughout the 100ns simulation run. Hydrogen bonds are a stronger and more stable type of interaction which determines the stability and binding affinity of a ligand inside the binding pocket of a protein. Out of all the ligands, DK2_DRUG formed four hydrogen bonds for the most part of the trajectory and DK4_DRUG formed five to six hydrogen bonds being more stable than others. DK1_DRUG, DK3_DRUG and DK5_DRUG formed atleast three hydrogen bonds throughout the trajectory similar to BIBR1532. Hydrogen bond plots indicated all the drugs were stable in the binding pocket with at least three hydrogen bonds formed by all the of them throughout the trajectory.

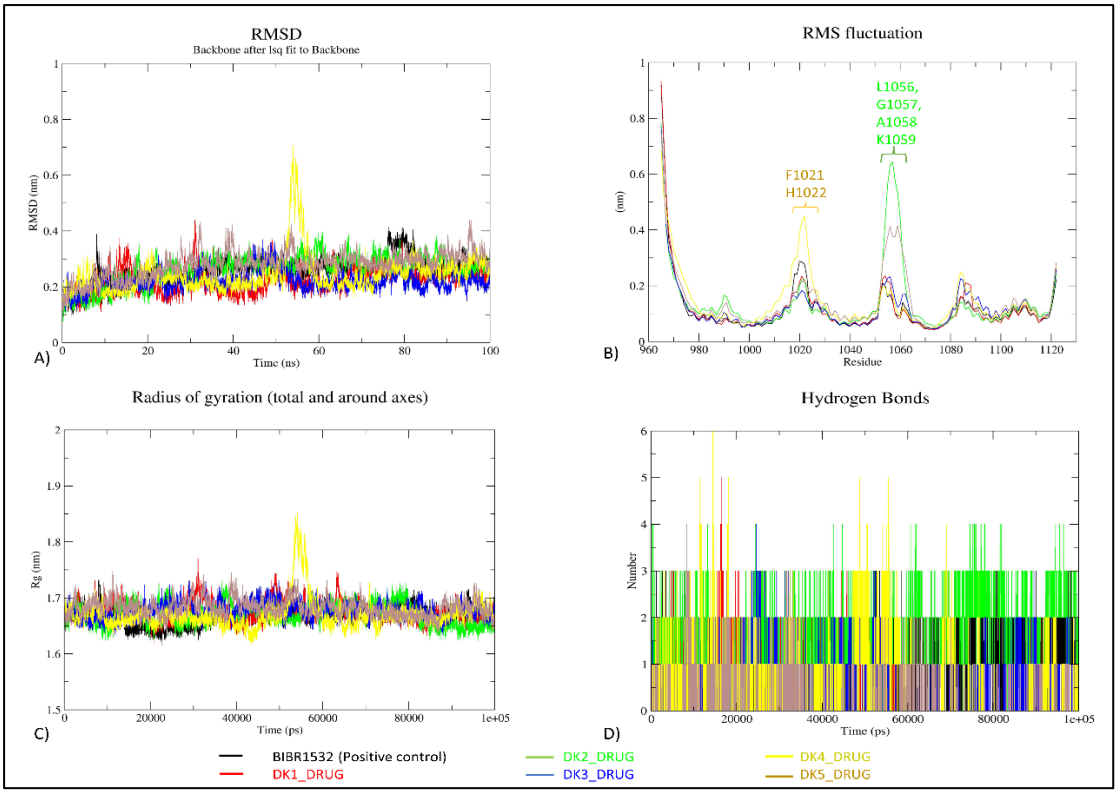

Figure.7: MD simulation plots for 100ns of top DrugBank hits in comparison with positive control BIBR1532 to investigate their stability in the bound state with hTERT thumb domain A) RMSD plot B) RMSF plot C) Radius of gyration plot D) Hydrogen bonds

4.10 MM-PBSA binding energy calculations

The binding free energies of all five top drugs and BIBR1532 were evaluated for the last 20ns trajectory to gain a better understanding of their stability and binding affinity in the thumb domain binding site. Both the MM-PBSA and MM-GBSA methods were employed to validate the consistency and reliability of the calculations. PB models are usually more accurate but computationally expensive, and GB models are faster but less accurate; however, both of them rely on different solvation models and hence can help us to cross-validate the results. All the top five drug-complexes and the positive control BIBR1532 exhibited negative effective binding energy in a similar pattern in the case of MM-PBSA and MM-GBSA calculations. This showed that all ligands were stable inside the binding pocket albiet to varying degrees. (**Figure.8**)
DK2_DRUG exhibited the most negative binding free energy of -53.01 kcal/mol better than the positive control BIBR1532 (-52.32 kcal/mol). DK3_DRUG, DK5_DRUG and DK4_DRUG also exhibited a negative binding free energy comparable to that of the positive control. DK1_DRUG exhibited the least binding free energy; however, it was still negative. A detailed analysis with energetic contribution of each type of polar and non-polar interaction to the effective binding free energy is given in **Table.3, Table.4, Figure.9 and Figure.10.**

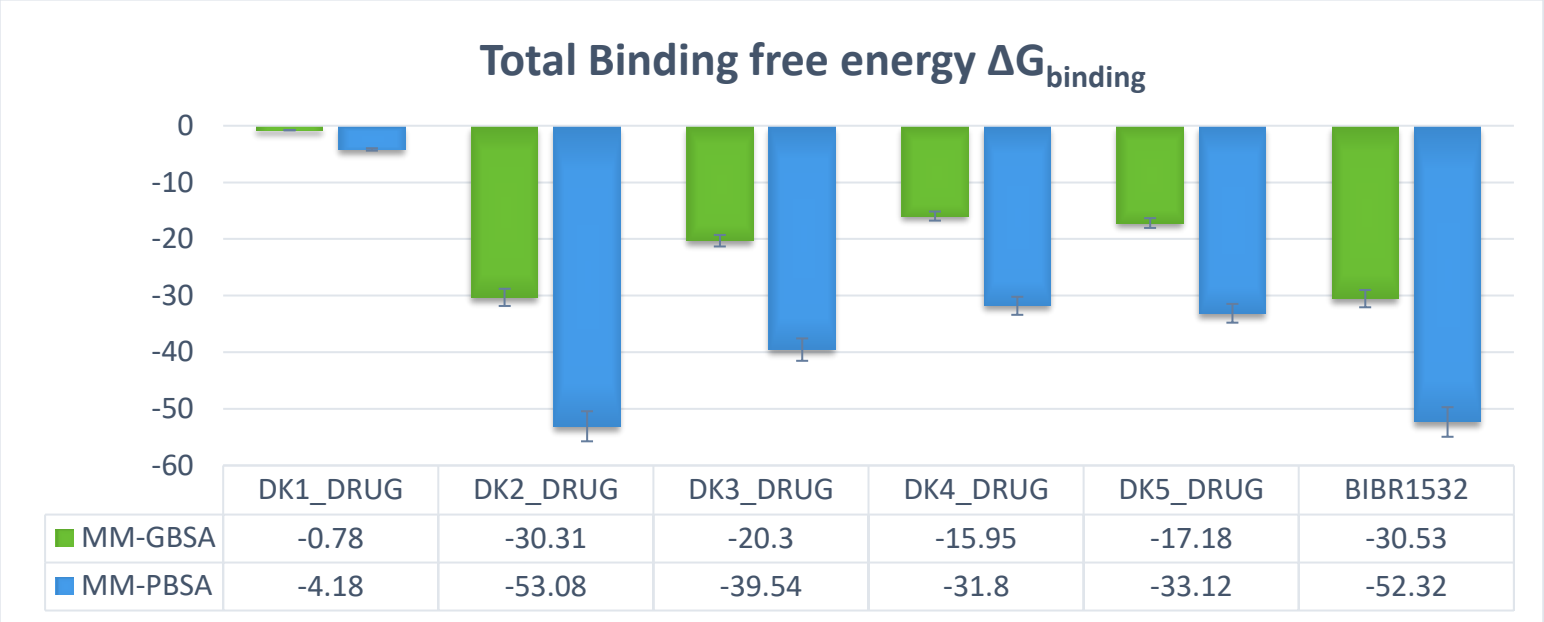

	DK1_DRUG	DK2_DRUG	DK3_DRUG	DK4_DRUG	DK5_DRUG	BIBR1532
MM-GBSA	-0.78	-30.31	-20.3	-15.95	-17.18	-30.53
MM-PBSA	-4.18	-53.08	-39.54	-31.8	-33.12	-52.32

Figure.8: Binding free energy calculations using MM-GBSA (green) and MM-PBSA (blue)

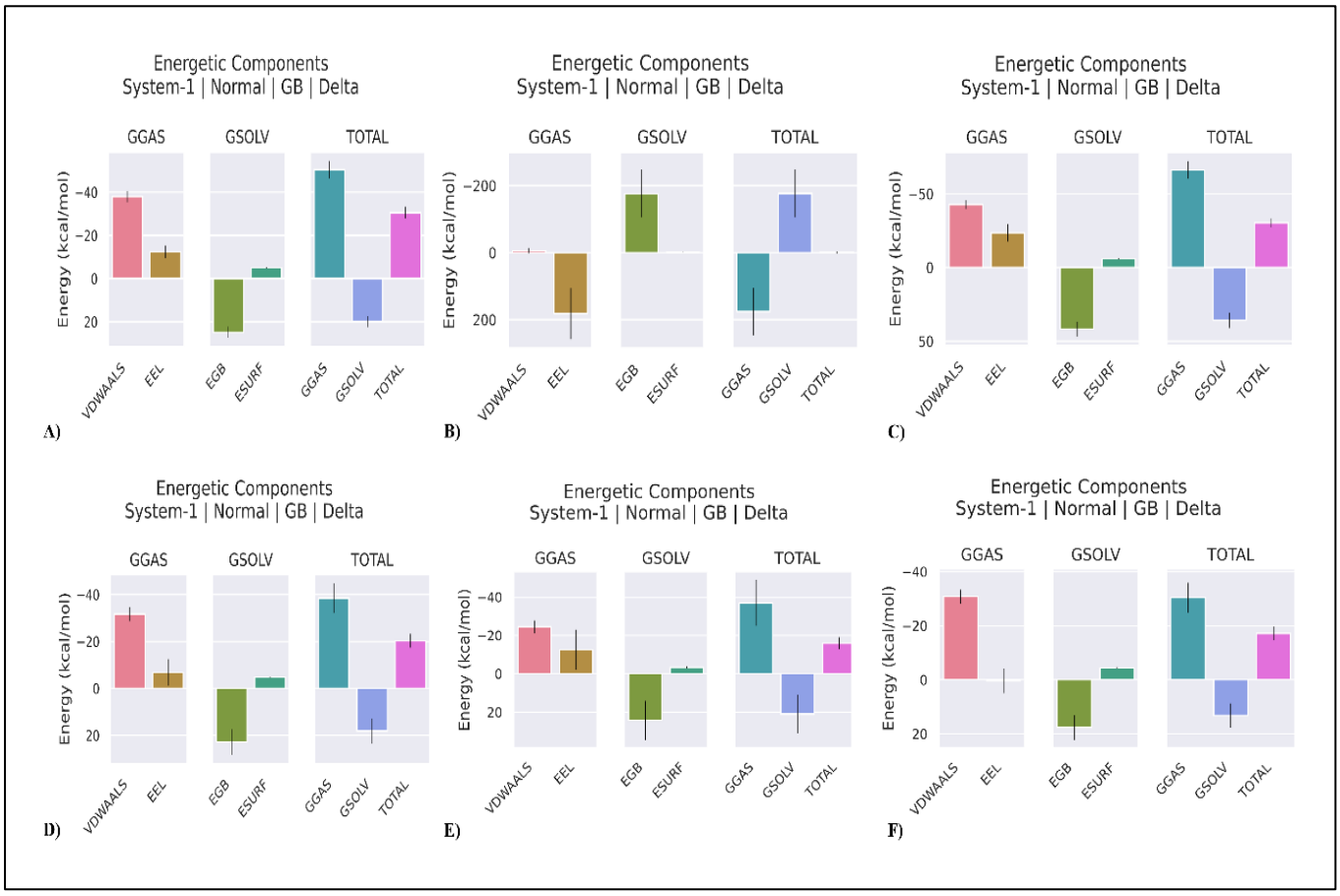

Figure.9: Binding free energy plots using MM-GBSA for A) BIBR1532 (control) B) DK1_DRUG C) DK2_DRUG D) DK3_DRUG E) DK4_DRUG F) DK5_DRUG

Table.3: MM-GBSA scores for top five drug candidates and positive control BIBR1532

Complex	BIBR1532 (Positive control)	DK1_DRUG	DK2_DRUG	DK3_DRUG	DK4_DRUG	DK5_DRUG
ΔE_{vdv}	-38.01	-6.00	-42.73	-31.65	-24.48	-30.77
ΔE_{elec}	-12.44	181.97	-23.46	-6.81	-12.49	0.39
ΔG_{GB}	24.87	-175.89	41.81	22.89	24.35	17.64
ΔG_{SA}	-4.95	-0.86	-5.93	-4.74	-3.33	-4.44
ΔG_{gas}	-50.45	175.97	-66.19	-38.45	-36.97	-30.38
ΔG_{sol}	19.92	-176.75	35.88	18.15	21.02	13.20
ΔG_{bind}	-30.53	-0.78	-30.31	-20.30	-15.95	-17.18
Total ± S.D	-30.53 ± 2.81	-0.78 ±3.58	-30.31 ±2.84	-20.30 ± 2.90	-15.95 ± 3.09	-17.18 ± 2.47

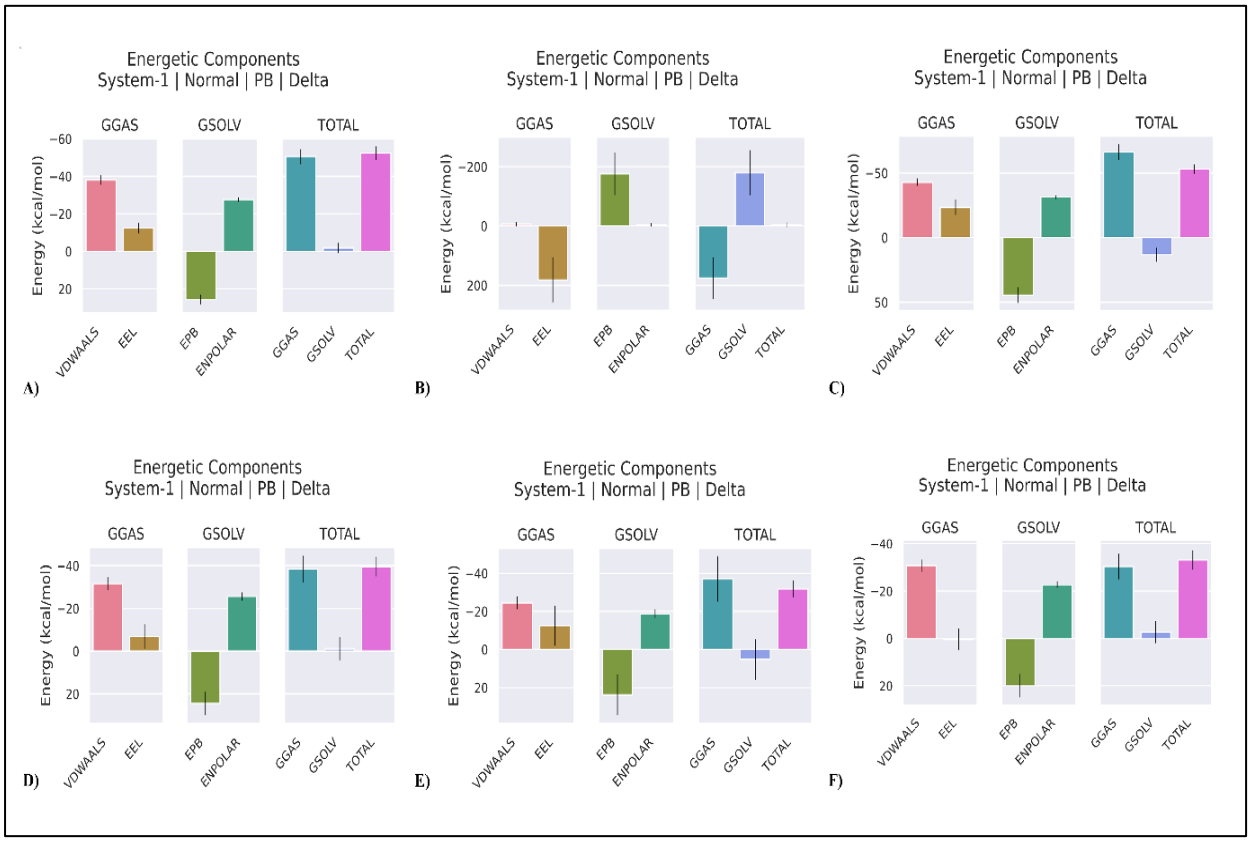

Figure 10: Binding free energy plots using MM-PBSA for A) BIBR1532 (control) B) DK1_DRUG C) DK2_DRUG D) DK3_DRUG E) DK4_DRUG F) DK5_DRUG

Table.4: MM-PBSA scores for top five drug candidates and positive control BIBR1532

Complex	BIBR1532 (Positive control)	DK1_DRUG	DK2_DRUG	DK3_DRUG	DK4_DRUG	DK5_DRUG
ΔE_{vdv}	-38.01	-6.00	-42.73	-31.65	-24.48	-30.77
ΔE_{elec}	-12.44	181.97	-23.46	-6.81	-12.49	0.39
ΔG_{PB}	25.72	-176.12	44.50	24.54	23.87	19.96
ΔG_{SA}	-27.59	-4.02	-31.32	-25.62	-18.70	-22.69
ΔG_{gas}	-50.45	175.97	-66.19	-38.45	-36.97	-22.69
ΔG_{sol}	-1.87	-180.15	13.18	-1.09	5.17	-2.74
ΔG_{bind}	-52.32	-4.18	-53.01	-39.54	-31.80	-33.12
Total ± S.D	-52.32 ± 3.57	-4.18 ±8.04	-53.01 ±3.84	-39.54 ± 4.53	-31.80 ±4.31	-33.12 ± 4.01

5. Discussion

The discovery of telomerase, an enzyme responsible for maintaining telomere length, has ignited substantial interest in its potential as a drug target with diverse implications in aging, cancer, and regenerative medicine (Fragkiadaki et al., 2022). Telomerase's indispensable role in countering telomere shortening and progression of almost 90% of cancer malignancies has positioned it as a promising target for innovative therapeutic strategies (Vishwakarma et al., 2023). Lack of availability of a structure since decades of its discovery has hindered the progress of structure-based drug designing of telomerase inhibitors.

In our study we have used the first ever reported structure of hTERT thumb domain (PDB ID: 5UGW) for designing inhibitors based on strong cues from literature about the binding of BIBR1532, a well-known and highly selective telomerase inhibitor in this domain (Hoffman et al., 2017).

Several studies have pointed out that BIBR1532 binds in a conserved hydrophobic and a clinically relevant FVYL pocket located in the thumb domain of tcTERT (Bryan et al., 2015; B. Liu et al., 2022).

Albeit preliminary studies also report that it binds in a similar manner in hTERT thumb domain but, a lack of co-crystalized structure of BIBR1532 with hTERT is a caveat in fully understand its exact binding site. Mutational studies and structural studies have confirmed that thumb domain is a contact point of P6.1 and CR4/5 loop of hTER in turn indicating a significant role of this domain in RNP assembly and enzymatic activity, making it a therapeutically strong target (Bryan et al., 2015; Hoffman et al., 2017).

In our study we have tried to exploit this pocket to firstly validate the exact binding site of BIBR1532 in hTERT thumb domain using a molecular dynamics approach. Based on this study, we have tried to repurpose selected lead drugs from DrugBank database as potential telomerase inhibitors. Results indicated that BIBR1532 shifted to an adjacent pocket 8.491 Å away instead of its putative FVYL pocket as in tcTERT but with strikingly conserved FVYL interactions. We have tried to validate the exact binding site of BIBR1532 using a two-way approach where we have generated two pharmacophore models for each of the two sites in the thumb domain and screened

them through DrugBank approved and investigational database for drug repurposing. We obtained negative results with Pharmacophore_A1 generated from putative FVYL pocket, as none of the screened and filtered compounds were able to dock there. On subsequent structural analysis and superimposition studies we observed that the pocket volume in hTERT with several protruding residues unlike in tcTERT was too small to accommodate any small molecule. (**Figure.5**)

Our study based on MD simulation and binding free energy calculations validated that the new pocket must be the actual binding site of BIBR1532 with conserved FVYL interactions here as well. Further, all the screened and filtered molecules from DrugBank approved and investigational databased using Pharmacophore_B1 were also able to dock onto this new pocket. Filtering was done in both the cases using druglikliness parameters like Lipinski's rule of 5, ADMET and TOPKAT. Finally, top lead drugs based on their mode of action, biological role and interaction with important residues in thumb domain were selected to finally validate their stability in the binding pocket of the protein using Molecular dynamics studies and binding free energy calculations.

To cross-validate our results, a 100ns MD simulation was performed for each of them in comparison to positive control BIBR1532 and their binding free energies were validated using MM-GBSA as well as MM-PBSA calculation. All five drugs DK1, DK2, DK3, DK4 and DK5 showed stable molecular dynamics trajectories based on parameters like RMSD, RMSF, RoG and H-bond analysis. Binding free energy calculations showed a similar pattern for all lead drugs using MM-GBSA and MM-PBSA, conclusively being negative for all. However, DK2_DRUG and DK3_DRUG showed maximum stability compared with BIBR1532.

In the current study, we have report the identification of five lead drugs from the DrugBank database that can be repurposed as telomerase inhibitors and used as potential anti-cancer therapeutics in future. Although further wet lab validation is required but these FDA Approved drugs have the potential to circumvent the traditional obstacles faced by conventional drug discovery processes, which cost millions of dollars and years of time. They also mark a paradigm shift, enabling the utilization of established compounds with a proven track record in terms of safety and efficacy to forever change the landscape of cancer therapeutics. Even if one of them shows potent inhibition and successfully validated in clinical studies, it will lead to a remarkable and accelerated emergence of anti-cancer drug. The drugs have a potential to even work for other diseases like diabetes in addition to cancer which have reported increase in the telomerase activity as one of their biomarkers. This study provides an impetus for future research into novel compounds capable of inhibiting telomerase and developing anticancer therapeutics.

Impact of the research in the advancement of knowledge or benefit to mankind

Cancer's devastating impact on human lives is a pressing global concern, claiming a staggering number of deaths each year. Among the many avenues explored for its treatment, targeting telomerase has emerged as a promising strategy due to its pivotal role in cancer's relentless growth. Telomerase is an established hallmark in more than 85% of cancer malignancies with a noticeable absence in somatic cells making it an attractive target. This is a major advantage of developing telomerase-targeted therapies in comparison with conventional anti-cancer therapies, such as chemotherapy and radiotherapy.

However, the **lack of approved small-molecule inhibitors**, rooted in the structural ambiguity of telomerase, has impeded drug development for decades. This critical knowledge gap has posed a significant roadblock, thwarting the development of novel anticancer therapies and perpetuating the urgent need for a breakthrough. Herein lies the **transformative potential of drug repurposing**, a groundbreaking approach used by us to **harness the anti-cancer potential of FDA-approved drugs** as telomerase inhibitors amidst the challenging landscape of discovering a toxicologically safe and potent drug. This strategy not only circumvents traditional obstacles but also accelerates the advancement of knowledge and offers tangible benefits to humanity.

As one of objectives of our study, we have tried to establish the exact binding site of a well-known and highly selective telomerase inhibitor named BIBR1532. This inhibitor is extensively used in several biochemical, kinetic, and in vivo studies but its exact binding site is still inconclusive due to the lack of a co-crystalized structure with the enzyme. Our research study involving a synergistic computational approach based on molecular dynamics has attempted to validate its exact binding site in the first reported crystal structure of the hTERT thumb domain, in context with previously reported preliminary studies.

We identified a new binding pocket in the hTERT thumb domain, wherein BIBR1532 binds however, surprisingly sharing the similar interactions with mutationally relevant residues, as reported previously. This new pocket was exploited by us using an in-silico drug designing approach to identify lead drug molecules from the DrugBank database containing FDA approved drugs. Such compounds targeting the thumb domain of the enzyme has a direct potential to inhibit the catalytic function of the enzyme and ultimately restriction of tumour cell replication potential.

We have identified five such lead drug molecules as potential telomerase inhibitors highlighting their promise in a new therapeutic context. Currently used for various conditions including hypertension, thrombosis, immune thrombocytopenia, actinic keratosis, and these drugs could be patented for a new anti-cancer regimen upon successful clinical validation. The study also opens up a large avenue to explore this domain to discover potent novel compounds based on similar scaffolds and mode of action. Such modified drugs stemming from the same scaffold can provide intellectual property rights and financial benefits as well.

Our research bridges the gap between existing FDA-approved drugs and their untapped potential as telomerase inhibitors. The impact of our research reverberates with human-centric benefits that extend far beyond the laboratory. By repurposing drugs with established

safety profiles, **we accelerate the journey from bench to bedside, saving invaluable time and resources.** This approach minimizes the risks of failure often associated with traditional drug development, ultimately expediting the availability of effective therapies to patients in dire need. While further evaluation through rigorous in-vitro and ex-vivo assays is needed, the implications of our discovery are far-reaching. Successfully establishing even one of the repurposed drugs as a potent telomerase inhibitor could catalyse a cascade of benefits in cancer treatment. It will moreover, **also lead to accessible and affordable availability of these drugs bridging the healthcare disparities and ensuring that even marginalized populations can access cutting-edge therapies.**

Future directions:

We are already working in the direction of discovering novel compounds using this study as a launch pad as potent telomerase inhibitors and validate them in vitro. The recent discovery of the full-length Cryo-EM structure of telomerase has opened up a larger avenue for the structure-based drug discovery of telomerase inhibitors. Moreover, the impact of our research work extends to other diseases beyond cancer, where escalated telomerase activity is documented, warranting exploration in diverse therapeutic contexts. This interdisciplinary approach holds the potential to revolutionize not only cancer treatment but various other medical fields as well, ushering in a new era of targeted therapies and improved patient outcomes.

I would also like to emphasize that this research work has also been recognized and awarded internationally by the European Molecular Biology Laboratory (EMBO) to be presented at an international conference on "Telomere function and evolution in health and disease," held in Portugal from 26th September to 1st October, 2022.

Literature References:

Brooks, B. R., Brooks, C. L., Mackerell, A. D., Nilsson, L., Petrella, R. J., Roux, B., Won, Y., Archontis, G., Bartels, C., Boresch, S., Caflisch, A., Caves, L., Cui, Q., Dinner, A. R., Feig, M., Fischer, S., Gao, J., Hodoscek, M., Im, W., … Karplus, M. (2009). CHARMM: The biomolecular simulation program. *Journal of Computational Chemistry*, *30*(10), 1545–1614. https://doi.org/10.1002/jcc.21287

Bryan, C., Rice, C., Hoffman, H., Harkisheimer, M., Sweeny, M., & Skordalakes, E. (2015). Structural Basis of Telomerase Inhibition by the Highly Specific BIBR1532. *Structure (London, England : 1993)*, *23*(10), 1934–1942. https://doi.org/10.1016/j.str.2015.08.006

Ding, X., Cheng, J., Pang, Q., Wei, X., Zhang, X., Wang, P., Yuan, Z., & Qian, D. (2019). BIBR1532, a Selective Telomerase Inhibitor, Enhances Radiosensitivity of Non-Small Cell Lung Cancer Through Increasing Telomere Dysfunction and ATM/CHK1 Inhibition. *International Journal of Radiation Oncology*Biology*Physics*, *105*(4), 861–874. https://doi.org/10.1016/j.ijrobp.2019.08.009

Essmann, U., Perera, L., Berkowitz, M. L., Darden, T., Lee, H., & Pedersen, L. G. (1995). A smooth particle mesh Ewald method. *The Journal of Chemical Physics*, *103*(19), 8577–8593. https://doi.org/10.1063/1.470117

Fragkiadaki, P., Renieri, E., Kalliantasi, K., Kouvidi, E., Apalaki, E., Vakonaki, E., Mamoulakis, C., Spandidos, D. A., & Tsatsakis, A. (2022). Telomerase inhibitors and activators in aging and cancer: A systematic review. *Molecular Medicine Reports*, *25*(5), 158. https://doi.org/10.3892/mmr.2022.12674

Gagnon, J. K., Law, S. M., & Brooks, C. L. (2016). Flexible CDOCKER: Development and application of a pseudo-explicit structure-based docking method within CHARMM.

Journal of Computational Chemistry, *37*(8), 753–762. https://doi.org/10.1002/jcc.24259

Ghanim, G. E., Fountain, A. J., van Roon, A.-M. M., Rangan, R., Das, R., Collins, K., & Nguyen, T. H. D. (2021). Structure of human telomerase holoenzyme with bound telomeric DNA. *Nature*, *593*(7859), Article 7859. https://doi.org/10.1038/s41586-021-03415-4

Grace Home. (n.d.). Retrieved May 11, 2023, from https://plasma-gate.weizmann.ac.il/Grace/

Hanwell, M. D., Curtis, D. E., Lonie, D. C., Vandermeersch, T., Zurek, E., & Hutchison, G. R. (2012). Avogadro: An advanced semantic chemical editor, visualization, and analysis platform. *Journal of Cheminformatics*, *4*(1), 17. https://doi.org/10.1186/1758-2946-4-17

Hoffman, H., Rice, C., & Skordalakes, E. (2017). Structural Analysis Reveals the Deleterious Effects of Telomerase Mutations in Bone Marrow Failure Syndromes. *The Journal of Biological Chemistry*, *292*(11), 4593–4601. https://doi.org/10.1074/jbc.M116.771204

Jha, P., Saluja, D., & Chopra, M. (2022). Structure-guided pharmacophore based virtual screening, docking, and molecular dynamics to discover repurposed drugs as novel inhibitors against endoribonuclease Nsp15 of SARS-CoV-2. *Journal of Biomolecular Structure & Dynamics*, 1–11. https://doi.org/10.1080/07391102.2022.2079561

Kant, R., Jha, P., Saluja, D., & Chopra, M. (2022). Identification of novel inhibitors of Neisseria gonorrhoeae MurI using homology modeling, structure-based pharmacophore, molecular docking, and molecular dynamics simulation-based approach. *Journal of Biomolecular Structure & Dynamics*, 1–14. https://doi.org/10.1080/07391102.2022.2121943

Kim, N. W., Piatyszek, M. A., Prowse, K. R., Harley, C. B., West, M. D., Ho, P. L., Coviello, G. M., Wright, W. E., Weinrich, S. L., & Shay, J. W. (1994). Specific association of

human telomerase activity with immortal cells and cancer. *Science (New York, N.Y.)*, *266*(5193), 2011–2015. https://doi.org/10.1126/science.7605428

Liu, B., He, Y., Wang, Y., Song, H., Zhou, Z. H., & Feigon, J. (2022). Structure of active human telomerase with telomere shelterin protein TPP1. *Nature*, *604*(7906), 578–583. https://doi.org/10.1038/s41586-022-04582-8

Liu, X., Ouyang, S., Yu, B., Liu, Y., Huang, K., Gong, J., Zheng, S., Li, Z., Li, H., & Jiang, H. (2010). PharmMapper server: A web server for potential drug target identification using pharmacophore mapping approach. *Nucleic Acids Research*, *38*(suppl_2), W609–W614. https://doi.org/10.1093/nar/gkq300

Meibohm, B., & Derendorf, H. (1997). Basic concepts of pharmacokinetic/pharmacodynamic (PK/PD) modelling. *International Journal of Clinical Pharmacology and Therapeutics*, *35*(10), 401–413.

Miller, B. R. I., McGee, T. D. Jr., Swails, J. M., Homeyer, N., Gohlke, H., & Roitberg, A. E. (2012). MMPBSA.py: An Efficient Program for End-State Free Energy Calculations. *Journal of Chemical Theory and Computation*, *8*(9), 3314–3321. https://doi.org/10.1021/ct300418h

Nguyen, T. H. D., Tam, J., Wu, R. A., Greber, B. J., Toso, D., Nogales, E., & Collins, K. (2018). Cryo-EM structure of substrate-bound human telomerase holoenzyme. *Nature*, *557*(7704), 190–195. https://doi.org/10.1038/s41586-018-0062-x

Pucci, C., Martinelli, C., & Ciofani, G. (2019). Innovative approaches for cancer treatment: Current perspectives and new challenges. *Ecancermedicalscience*, *13*, 961. https://doi.org/10.3332/ecancer.2019.961

Rao, S. N., Head, M. S., Kulkarni, A., & LaLonde, J. M. (2007). Validation Studies of the Site-Directed Docking Program LibDock. *Journal of Chemical Information and Modeling*, *47*(6), 2159–2171. https://doi.org/10.1021/ci6004299

Rarey, M., Kramer, B., Lengauer, T., & Klebe, G. (1996). A fast flexible docking method using an incremental construction algorithm. *Journal of Molecular Biology*, *261*(3), 470–489. https://doi.org/10.1006/jmbi.1996.0477

Robart, A. R., & Collins, K. (2011). Human telomerase domain interactions capture DNA for TEN domain-dependent processive elongation. *Molecular Cell*, *42*(3), 308–318. https://doi.org/10.1016/j.molcel.2011.03.012

Shay, J. W. (1997). Telomerase in human development and cancer. *Journal of Cellular Physiology*, *173*(2), 266–270. https://doi.org/10.1002/(SICI)1097-4652(199711)173:2<266::AID-JCP33>3.0.CO;2-B

Shay, J. W., & Wright, W. E. (2000). Hayflick, his limit, and cellular ageing. *Nature Reviews. Molecular Cell Biology*, *1*(1), 72–76. https://doi.org/10.1038/35036093

Valdés-Tresanco, M. S., Valdés-Tresanco, M. E., Valiente, P. A., & Moreno, E. (2021). gmx_MMPBSA: A New Tool to Perform End-State Free Energy Calculations with GROMACS. *Journal of Chemical Theory and Computation*, *17*(10), 6281–6291. https://doi.org/10.1021/acs.jctc.1c00645

Vanommeslaeghe, K., Hatcher, E., Acharya, C., Kundu, S., Zhong, S., Shim, J., Darian, E., Guvench, O., Lopes, P., Vorobyov, I., & MacKerell, A. D. (2010). CHARMM General Force Field (CGenFF): A force field for drug-like molecules compatible with the CHARMM all-atom additive biological force fields. *Journal of Computational Chemistry*, *31*(4), 671–690. https://doi.org/10.1002/jcc.21367

Vařeková, R. S., Koča, J., & Zhang, C.-G. (2004). Complexity and Convergence of Electrostatic and van der Waals Energies within PME and Cutoff Methods. *International Journal of Molecular Sciences*, *5*(4), Article 4. https://doi.org/10.3390/i5040154

Vishwakarma, K., Dey, R., & Bhatt, H. (2023). Telomerase: A prominent oncological target for development of chemotherapeutic agents. *European Journal of Medicinal Chemistry*, *249*, 115121. https://doi.org/10.1016/j.ejmech.2023.115121

Wang, E., Sun, H., Wang, J., Wang, Z., Liu, H., Zhang, J. Z. H., & Hou, T. (2019). End-Point Binding Free Energy Calculation with MM/PBSA and MM/GBSA: Strategies and Applications in Drug Design. *Chemical Reviews*, *119*(16), 9478–9508. https://doi.org/10.1021/acs.chemrev.9b00055

Wishart, D. S., Knox, C., Guo, A. C., Cheng, D., Shrivastava, S., Tzur, D., Gautam, B., & Hassanali, M. (2008). DrugBank: A knowledgebase for drugs, drug actions and drug targets. *Nucleic Acids Research*, *36*(Database issue), D901–D906. https://doi.org/10.1093/nar/gkm958

Wright, W. E., & Shay, J. W. (1992). The two-stage mechanism controlling cellular senescence and immortalization. *Experimental Gerontology*, *27*(4), 383–389. https://doi.org/10.1016/0531-5565(92)90069-c

Wu, G., Robertson, D. H., Brooks III, C. L., & Vieth, M. (2003). Detailed analysis of grid-based molecular docking: A case study of CDOCKER—A CHARMm-based MD docking algorithm. *Journal of Computational Chemistry*, *24*(13), 1549–1562. https://doi.org/10.1002/jcc.10306